CrossMark

CAMBRIDGE
UNIVERSITY PRESS

RESEARCH ARTICLE

Improving measurement performance via fusion of classical and quantum accelerometers

Xuezhi Wang,[1]* Allison Kealy,[1] Christopher Gilliam,[2,5] Simon Haine,[3] John Close,[3] Bill Moran,[4] Kyle Talbot,[1] Simon Williams,[4] Kyle Hardman,[3] Chris Freier,[3] Paul Wigley,[3] Angela White,[3] Stuart Szigeti,[3] and Sam Legge[3]

[1] School of Science, RMIT University, Melbourne, Australia

[2] School of Engineering, RMIT University, Melbourne, Australia

[3] Department of Quantum Science, Research School of Physics, Australia National University, Canberra, Australia

[4] School of Engineering, University of Melbourne, Melbourne, Australia

[5] School of Engineering, University of Birmingham, Birmingham, UK.

*Corresponding author. E-mail: xuezhi.wang@rmit.edu.au

Abstract

While quantum accelerometers sense with extremely low drift and low bias, their practical sensing capabilities face at least two limitations compared with classical accelerometers: a lower sample rate due to cold atom interrogation time; and a reduced dynamic range due to signal phase wrapping. In this paper, we propose a maximum likelihood probabilistic data fusion method, under which the actual phase of the quantum accelerometer can be unwrapped by fusing it with the output of a classical accelerometer on the platform. Consequently, the recovered measurement from the quantum accelerometer is used to estimate bias and drift of the classical accelerometer which is then removed from the system output. We demonstrate the enhanced error performance achieved by the proposed fusion method using a simulated 1D accelerometer precision test scenario. We conclude with a discussion on fusion error and potential solutions.

1. Introduction

Initially demonstrated by Carnal and Mlynek (1991) and Keith et al. (1991), quantum accelerometers based on cold atom interferometry generate high precision measurements with extremely low drift over a long time period (Kitching et al., 2011; Degen et al., 2017; Bongs et al., 2019). Laboratory experiments demonstrate the accuracy of cold atom accelerometers to be fifty times greater than that of their classical counterparts (Jekeli, 2005; Hardman et al., 2016). More recently, a three-dimensional quantum accelerometer was implemented by Battelier et al. (2020). This makes cold atom sensors potentially well suited to inertial navigation systems, where the bias and drift of accelerometers and gyroscopes has a direct impact on the quality of positioning and attitude.

To deploy quantum sensors for inertial navigation, one has to solve several engineering problems such as large weight and size, the requirement of sophisticated cryogenic devices to run, etc. In addition, at least two technical challenges must be resolved (Canciani, 2012). First, the nature of cold atom interferometry is such that the resulting sample rate is typically below 10 Hz. A lower sample rate will result in a higher achievable measurement accuracy (Peters et al., 2001; Hardman et al., 2016). This sample rate is significantly lower than existing classical accelerometers, which can operate at

frequencies of the order of 800 Hz. Second, the dynamic range of quantum accelerometers is very low, typically reported below $1 \times 10^{-2}\,\mathrm{m\,s^{-2}}$ (Gillot et al., 2014; Freier et al., 2016). Fundamentally, the output signal of a quantum accelerometer is sinusoidal, with the body acceleration value proportional to the signal phase. When the body acceleration value is beyond the dynamic range, the output signal will be wrapped because of the circular phase of the sinusoidal wave. In this paper, we refer to this as the phase wrapping problem. Mathematically, this problem is referred to as the integer ambiguity resolution problem. Depending on actual applications, various approaches are available in the literature, such as the PPP RTK in GNSS positioning (Kim and Langley, 2000), frequency estimation (McKilliam et al., 2010) and distance estimation (Li et al., 2013) based on non-coherent radar signals. Similar to these applications, unwrapping the phase of the quantum accelerometer output signal will enable the underlying quantum accelerometer to gain an extended dynamic range.

The phase wrapping problem was addressed by Bonnin et al. (2018), who showed that implementing the simultaneous atom interferometers with different interrogation times could extend the dynamic range, whereas operating in phase quadrature improved the sensitivity. This approach increases the dynamic range of the quantum accelerometer at the cost of a more complicated hardware configuration. The work by Dutta et al. (2016) used joint interrogation to eliminate the dead times, i.e. the preparation time between two adjacent cold atom interferometric cycles.

A hybrid cold atom/mechanical accelerometer was considered by Lautier et al. (2014), where the atom interferometer signal phase is compensated by using the signal of a classical accelerometer. A similar idea was presented by Cheiney et al. (2018), where a hybrid system combines the outputs of quantum and mechanical accelerometers in an optimisation framework. An extended Kalman filter is used in the loop to estimate the bias and drift of a classical sensor as well as the phase of a quantum sensor. This results in a bandwidth of 400 Hz and a stability of 10 ng after 11 h of integration by the hybrid sensor. This work is extended to a three-axis implementation by Battelier et al. (2020). The accuracy of the quantum accelerometer was tested only in the range of $0\sim100\,\mu g$ and simultaneously estimating the quantum sensor phase and classical sensor bias is nontrivial. Both the above two approaches are related to our work in the sense of estimating the phase of a quantum accelerometer but differ in the ways of phase unwrapping and how the classical sensor bias is estimated and removed. More recent work by Tennstedt and Schön (2020) investigates the possibility of using the measurement of a cold atom interferometer sensor in Mach–Zehnder configuration in a navigation solution. They combine the cold atom sensor measurement with classical inertial sensors via a filter solution, observing an improved navigation performance when the underlying acceleration is small.

As mentioned above, existing efforts to extend the dynamic range of a quantum accelerometer essentially involves modifying the hardware configuration, which is nontrivial. In this paper, we propose a maximum likelihood probabilistic data fusion method that uses the accuracy of the quantum accelerometer – operating at a low sample rate – to re-calibrate a classical accelerometer over its full dynamic range. Our approach uses standard signal processing techniques and improves the inertial navigation capabilities of classical accelerometers without the need to extend the dynamic range of the quantum accelerometer. The idea is to unwrap the phase of the quantum accelerometer output signal by fusing the acceleration measurement of the classical sensor into the quantum sensor model at the quantum sensor sample rate.

The paper is arranged as follows. The problem statement and fusion idea are described in Section 2. The approach for quantum sensor signal phase unwrapping using a classical accelerometer via maximum likelihood estimation is presented in Section 3. The performance of the proposed method is demonstrated by simulation results in a 1D inertial navigation scenario in Section 4, which is followed by the conclusions in Section 5.

2. Limitations of quantum accelerometers

A quantum accelerometer operates by transforming a cloud of cold atoms into two spatially separated clouds in free fall such that the change of their vertical displacement in time mimics the two arms of

an interferometer. The manipulation of the atom cloud is achieved by using one laser pulse to split the cloud and then a second to recombine the cloud. When the sensor has been subject to a specific force (e.g. acceleration and/or gravity), the two clouds of atoms exhibit different phase characteristics that can be measured. Counting the number of atoms in each cloud yields the relative phase, which in turn yields the specific force of the platform relative to the inertial frame defined by the freely falling atoms. Such a sensor has the potential to produce very precise measurements of acceleration or gravity (Freier et al., 2016; Ménoret et al., 2018). However, the sensor suffers from two key limitations that must be overcome.

The first challenge is that, in general, the quantum sensor has a low sampling rate that is governed by two features: the time required to produce a cloud of cold atoms; and the time that the atoms spend in free fall. A larger size of the atom cloud and a longer time these atoms spend in free fall will result in a better precision of the acceleration measurement. A trade-off therefore exists between the performance of the sensor and the time between measurements. Some laboratories are exploring this trade-off to enable sample rates of up to 330 Hz (Butts et al., 2011; McGuinness et al., 2012).

The second challenge the sensor faces is a low dynamic range. Let T be half the total interrogation time of the sensor, which is equivalent to half the time of flight for the atoms. For a constant acceleration a, the phase shift between the two atom clouds is (Peters et al., 2001)

$$\triangle\phi = k_{\text{eff}}aT^2, \tag{2.1}$$

where the effective wavenumber is $k_{\text{eff}} \approx 4\pi/\lambda$ and λ is the wavelength of the laser. This phase shift is measured by the cold atom accelerometer as

$$S = N \sin(k_{\text{eff}}aT^2 + \phi_0), \tag{2.2}$$

where N is the number of atoms in the atomic cloud and ϕ_0 is the initial phase. Given S, an acceleration measurement is thus obtained by inverting Equation (2.2). However, although a single acceleration a uniquely determines S, the reverse is not true; a given S can be obtained from distinct accelerations a. Figure 1 illustrates the relationship in Equation (2.2) with $N = 1{,}000$ atoms, $\lambda = 780$ nm, $T = 1$ ms and a laser pulse width of $\tau = 1\,\mu$s.[1] We see that once the acceleration exceeds $\pm 0{\cdot}05$ m s^{-1}, an ambiguity occurs, and multiple accelerations map to the same S/N value indicated by the black dashed line.

In this work, we are interested in unwrapping the phase of the accelerometer output S to identify the underlying acceleration a. In Section 3, we introduce an algorithm that performs this unwrapping by fusing a classical sensor with a quantum sensor. The resulting algorithm overcomes both the low sampling rate and low dynamic range challenges exhibited by the quantum sensor.

3. Phase unwrapping by data fusion

In this section, we introduce our approach to unwrapping the phase of the quantum accelerometer via fusion with a classical accelerometer.[2] We assume that the classical accelerometer is perfectly aligned with the quantum accelerometer. Based on Equation (2.2), we can write a complete noise-free quantum accelerometer measurement model as follows (Bonnin et al., 2018):

$$a = f(S, s, n)$$
$$= \begin{cases} \dfrac{s}{k_{\text{eff}}T^2}\left[\arcsin\left(\dfrac{S}{N}\right) + 2n\pi + \phi_0\right], & s = 1; \\[3mm] \dfrac{s}{k_{\text{eff}}T^2}\left[\arcsin\left(\dfrac{S}{N}\right) - (2n+1)\pi - \phi_0\right], & s = -1, \end{cases} \tag{3.1}$$

---

[1] τ is the pulse width of the beam splitter in the Mach–Zehnder interferometer. Ideally, Equation (2.1) holds if $\tau \ll T$.
[2] This assumption may never hold for a real system. Nevertheless, the misalignment angles can be estimated and used to correct the system via Kalman filters.
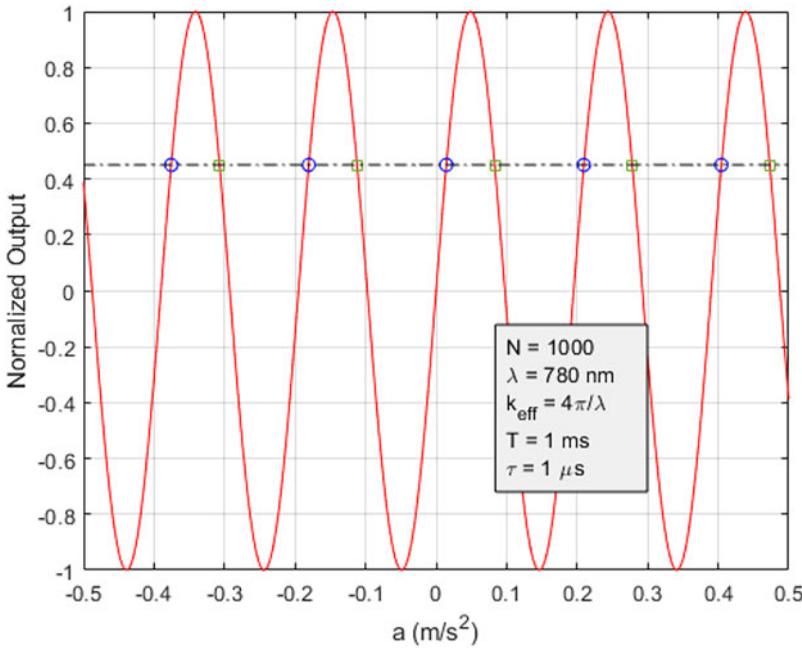
Figure 1. *Normalised output signal (S/N) of the quantum accelerometer as a function of input a. An output signal (black dashed line) corresponds with multiple acceleration values as indicated by blue circles and dark green boxes, which may be the underlying acceleration measured.*

where $s = \pm1$ is the sign function and $n \in \mathbb{Z}$ is an integer. In the presence of shot noise, to a good approximation, this gives a signal model of the form (Close et al., 2019)

$$a_q = f(S, s, n) + v_q, \tag{3.2}$$

where $v_q \sim \mathcal{N}(0, \sigma_q^2)$, $\mathcal{N}(a, b)$ stands for a Gaussian distribution with mean a, variance b and $\sigma_q = 1/(k_{\text{eff}}T^2\sqrt{N})$ signifies the measurement noise dominated by shot noise which is consistent with the experimental result reported by Cheinet et al. (2008). Note that the two solution sets to Equation (3.1) are indicated by the green and blue circles in Figure 1. Accordingly, to obtain the unwrapped acceleration, we need to determine which equation to use and estimate the integer n.

We solve this dual estimation problem through fusion with a classical accelerometer. Our fusion algorithm is based on the maximum likelihood estimation and comprises two steps. First, using the classical specific force measurement a_c and the output of the cold atom sensor S, a rough estimate of n is obtained by inverting Equation (3.1) as follows:

$$\hat{n}_1 = \frac{k_{\text{eff}}T^2}{2\pi}a_c - \frac{1}{2\pi}\left(\arcsin\left(\frac{S}{N}\right) - \phi_0\right), \tag{3.3a}$$

$$\hat{n}_2 = \frac{k_{\text{eff}}T^2}{2\pi}a_c + \frac{1}{2\pi}\left(\arcsin\left(\frac{S}{N}\right) - \phi_0\right) - \frac{1}{2}. \tag{3.3b}$$

Note that $\hat{n}_1$ and $\hat{n}_2$ are rounded to the nearest integer. Second, the ambiguity-corrected quantum acceleration a_q is obtained by evaluating Equation (3.1) for a finite set of integers centred around $\hat{n}_1$ and $\hat{n}_2$, and choosing the specific force value closest to a_c in the maximum likelihood sense. The initial phase ϕ_0 is a known constant determined by the hardware configuration. For simplicity, unless stated otherwise, we shall henceforth assume that $\phi_0 = 0$. It is worth mentioning that a poor signal sensitivity with respect to the underlying acceleration occurs near the peaks of the sinusoid (see Figure 1), which

may lead large estimation error in Equation (3.3), and we will discuss this more toward the end of Section 4.

While the phase unwrapping using data from a classical accelerometer provides the fusion output of quantum grade accuracy, the data are only available at the sampling rate of quantum accelerometer, which is much lower than that of a high-end classical accelerometer. One way to solve this problem and obtain quantum grade data at the rate of classical data is to estimate the slow varying bias term by filtering, which is observable from the fusion output data. In this work, a simple error state Kalman filter is used for estimating the bias of classical accelerometer data. The fusion process at time t_k, based on a maximum likelihood estimation approach, is specifically given by the following steps.

1. Input: $a_c(k)$ from classical accelerometer; S_k from quantum accelerometer.
2. Maximum likelihood method for parameter estimation:

$$(n_k^o, s_k^o) = \arg \max_{n_k \in \mathbb{Z}, s_k \pm 1} p(a_q(k) \,|\, S_k, a_c(k)), \tag{3.4}$$

where, following Equation (3.3),

$$n_k^o = \begin{cases} \dfrac{k_{\text{eff}} T^2}{2\pi} a_c(k) - \dfrac{1}{2\pi} \arcsin\left(\dfrac{S_k}{N}\right), & s_k^o = 1; \\[3mm] \dfrac{k_{\text{eff}} T^2}{2\pi} a_c(k) + \dfrac{1}{2\pi} \arcsin\left(\dfrac{S_k}{N}\right) - \dfrac{1}{2}, & s_k^o = -1. \end{cases}$$

3. Estimate $a_f(k)$ using Equation (3.1), the ambiguity-corrected quantum acceleration output as shown in Figure 2, given S_k and n_k^o and s_k^o. Its conditional distribution is

$$a_q(k) \,|\, S_k, n_k^o, s_k^o \sim \mathcal{N}(a_q(k), \sigma_q^2),$$

where $\sigma_q = 1/(k_{\text{eff}} T^2 \sqrt{N})$.

4. Estimate measurement bias $\hat{b}(k)$ from $a_c(k)$. As shown in Figure 2, a simple error state Kalman filter (Groves, 2008) is adopted to estimate the bias of $a_c(k)$ based on the ambiguity-corrected quantum acceleration output a_q, which serves as the filtering measurement, at the sampling rate of quantum accelerometer.
5. The final fusion output $a_{\text{out}}(k)$ is given by

$$a_{\text{out}}(k) = a_c(k) - \hat{b}(k). \tag{3.5}$$

Figure 2 illustrates the above procedure based on the simulation scenario where the classical accelerometer sampling frequency is 200 Hz and quantum accelerometer sampling frequency is 1 Hz.

We now evaluate the performance of the proposed algorithm via Monte Carlo simulations under the condition that the dynamic range of ground truth acceleration is well beyond that of the quantum accelerometer but within that of the classical accelerometer (though this is impossible in practice). At each run, the data of ground truth acceleration are drawn from a uniform distribution. The following configuration for the cold atom sensor is used: $N = 10,000$ atoms, $T = 1$ ms half interrogation time, $\tau = 1\,\mu$s beam splitter pulse width of the laser and a laser wavelength of $\lambda = 780$ nm.

We assume that the output a_c of the classical accelerometer at t can be expressed as (Titterton and Weston, 2004):

$$a_c(t) = a(t) + b(t) + w(t), \tag{3.6}$$

where $a(t)$ signifies the true specific force, $b(t)$ represents measurement bias which is the sum of a constant bias term and a random bias term, the latter is modelled as a first-order Gauss–Markov process with time constant τ_a, and $w(t)$ represents the random errors associated with the sensor. Note that for this simulation, $b(t)$ may also include the accelerometer scale-factor error which has the effect similar
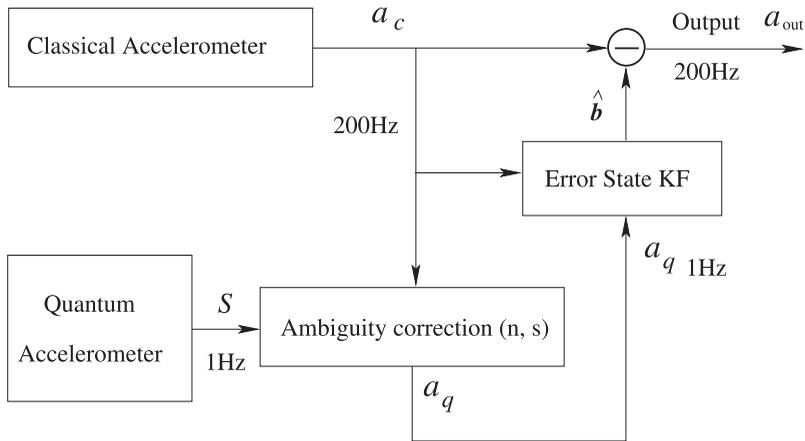
Figure 2. *Fusion of classical accelerometer and quantum accelerometer. Errors of the classical accelerometer are corrected using low rate quantum accelerometer measurements after ambiguity correction. The estimated (slow varying) bias term $\hat{b}$ of the classical accelerometer reading is obtained using an error state Kalman filter whose measurement is the signal difference $a_c - a_q$.*

to that of bias error, except that the error term increases as the input acceleration increases. In the simulation, both the constant bias and the standard deviation of random bias are set to $1 \times 10^{-3}\,\mathrm{m\,s^{-2}}$, and the time constant is $\tau_a = 2{,}000\,\mathrm{s}$, which is equivalent to the bias of a high-end tactical grade sensor (Chow, 2011). The random error of the accelerometer is assumed to be a zero-mean Gaussian random variable (Quinchia et al., 2013), i.e.

$$w(t) \sim \mathcal{N}(0, \sigma_c^2), \tag{3.7}$$

where $\sigma_c = 1{\cdot}4 \times 10^{-3}\,\mathrm{m\,s^{-2}}$ is the standard deviation.

The error statistics for this evaluation are shown in Figures 3 and 4, based on 10,000 Monte Carlo simulations. These histograms show the error between the ambiguity-corrected quantum acceleration estimate a_q and the original classical measurement a_c for two situations: the cold atom sensor with shot noise corruption (blue) and without (orange). In Figure 3, the classical acceleration is drawn from $\mathcal{U}(-10\,\mathrm{m\,s^{-2}}, 10\,\mathrm{m\,s^{-2}})$ whereas in Figure 4, the measurement is drawn from $\mathcal{U}(-1{,}000\,\mathrm{m\,s^{-2}}, 1{,}000\,\mathrm{m\,s^{-2}})$. We observe that the main contribution to the fusion error spread without shot noise (orange) is the nonlinear sensitivity of the mapping between the sensor output signal and the underlying acceleration in the low input dynamical acceleration range. We also observe that the spread of the fusion errors increases as the input acceleration dynamical range increases, because the maximum likelihood estimator error increases since the likelihood from Equation (3.4) becomes flat. This error is discussed further in Section 4.

In the next section, we demonstrate the performance of our fusion approach using simulations of a one-dimensional inertial navigation scenario.

4. Navigation simulation results

In this section, we evaluate the performance of the proposed fusion algorithm in the context of inertial navigation via Monte Carlo simulations. Practically, there are many error sources including those due to gravity, rotation of the earth and imperfect inertial sensors which will contribute to the acceleration, velocity and position errors of an inertial navigation system on a moving vehicle (Braasch, 2015). To concentrate on the accelerometer performance comparison, we will consider a one-dimensional inertial navigation case where the vehicle is on a perfectly flat, perfectly straight track and only the accelerometer is needed. Real examples of this are the rocket sleds which are used for testing equipment and various
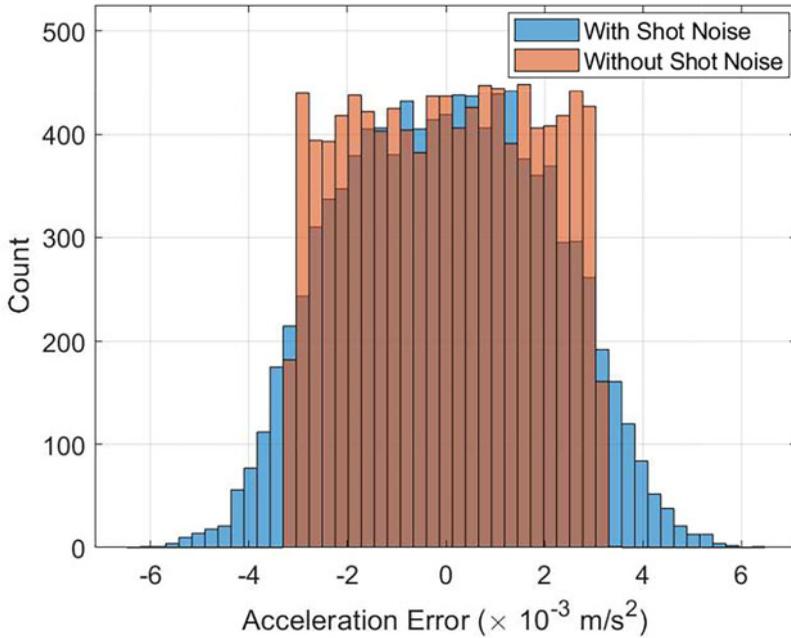
Figure 3. *Fusion error statistics ($a_q - a_c$) from 10,000 Monte Carlo runs for a drawn from $\mathcal{U}(-10\,\mathrm{m\,s}^{-2}, 10\,\mathrm{m\,s}^{-2})$ in the presence (blue) and absence (orange) of shot noise.*
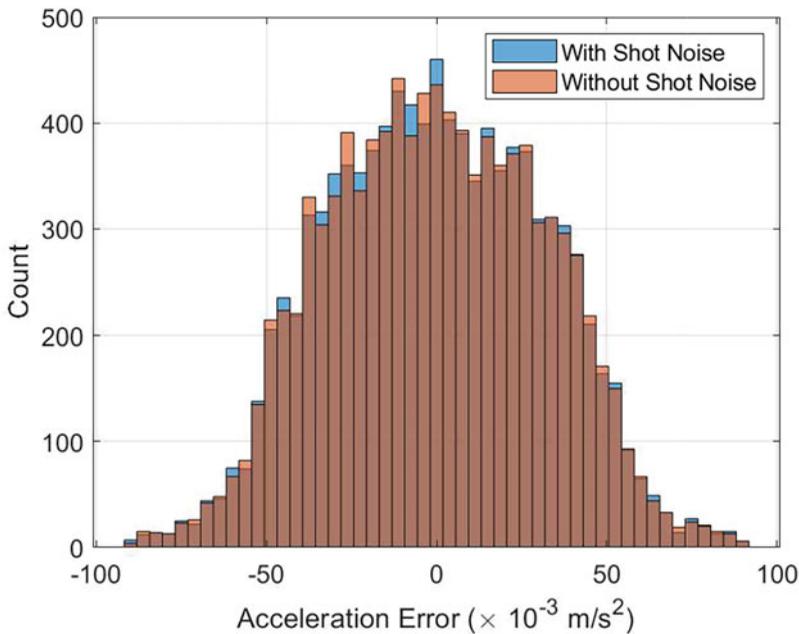

Figure 4. *Fusion error statistics ($a_q - a_c$) via 10,000 Monte Carlo runs for a drawn from $\mathcal{U}(-1{,}000\,\mathrm{m\,s}^{-2}, 1{,}000\,\mathrm{ms}^{-2})$ in the presence (blue) and absence (orange) of shot noise. This graph shows that for high input acceleration magnitude from the classical accelerometer, the fusion error distribution is dominated by the algorithm nonlinear sensitivity. Compared with Figure 3, the fusion error spread increases with the input acceleration dynamical range.*
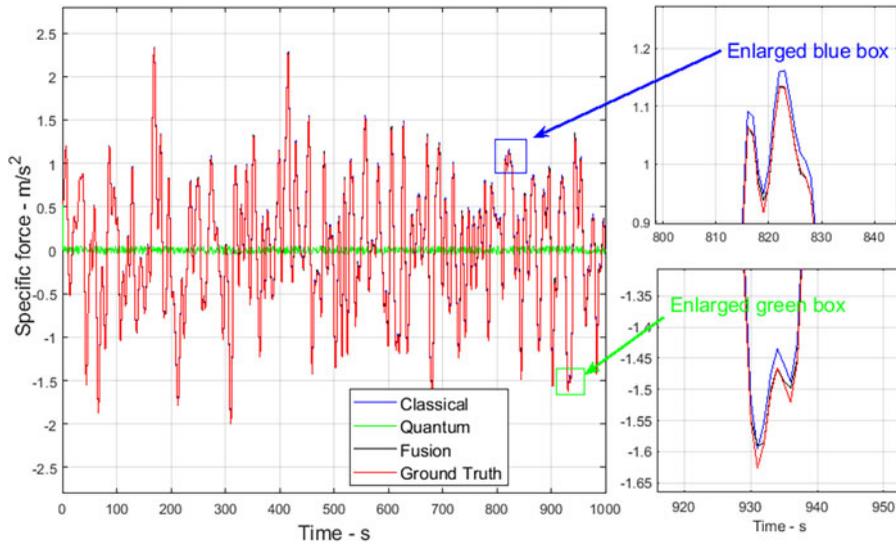
Figure 5. *Comparison of specific force values between classical, quantum, fusion and ground truth in a single run. Apart from the quantum accelerometer output which is indicated in green, the other three are overlapped in this figure. We highlight the RMS error difference between the classical and fusion in Figure 6.*

sensors. We idealise such a sled that moves in one dimension by assuming that the accelerometer is mounted in parallel to the track and ignoring sway and vibration, so that velocity is the result of integrating the specific force once and the distance along the track is obtained from an additional integration. Note that this is not a realistic scenario as even a nominally horizontal accelerometer will exhibit some sensitivity to the gravity reaction which we ignored here.

As shown in Figure 2, the system consists of a classical accelerometer and a quantum accelerometer. The initial position and velocity of the vehicle are set to zero. At each run, the underlying body specific force is randomly generated (a single realisation is shown in Figure 5), and its spectrum follows a zero-mean Gaussian distribution $a \sim \mathcal{N}(0, \sigma_a^2)$ with standard deviation $\sigma_a = 1\,\mathrm{m\,s^{-2}}$. For the classical accelerometer, the standard deviation of measurement noise is $\sigma_q = 1{\cdot}4 \times 10^{-3}\,\mathrm{m\,s^{-2}}$ and both the constant bias and the standard deviation of random bias in $b(t)$ are $1 \times 10^{-3}\,\mathrm{m\,s^{-2}}$. For the quantum accelerometer, we assume that its measurement noise is dominated by shot noise with distribution $v_f \sim \mathcal{N}(0, \sigma_s^2)$, where $\sigma_s = 1/(k_{\mathrm{eff}} T_{pi}^2 \sqrt{N})$, where the effective wavenumber is $k_{\mathrm{eff}} = 4\pi/\lambda$, $\lambda = 780\,\mathrm{nm}$, the half interrogation time $T = 1\,\mathrm{ms}$, the duration of the laser beam splitter is assumed to be $\tau = 1 \times 10^{-6}\,\mathrm{s}$ and the average number of atoms per shot is $N = 10{,}000$. Based on these parameters, we have $\sigma_s = 3{\cdot}1 \times 10^{-4}\,\mathrm{m\,s^{-2}}$ (note that the noise level is larger than the achievable value of $3 \times 10^{-8}\,\mathrm{m\,s^{-2}}$ mentioned by Jekeli, 2005; Cheiney et al., 2019). The sampling rate of the classical accelerometer is 200 Hz, while the quantum accelerometer is set at 1 Hz.

In this special inertial navigation scenario, we examine two cases. In the first, the computed inertial navigation is driven by the output of the classical accelerometer alone, and in the second, navigation is driven by the fusion of the classical with the quantum following the proposed fusion procedure, as illustrated in Figure 2. We compare the inertial navigation performance of the two cases in terms of root-mean-squared (RMS) errors.

Figure 5 shows a comparison of the estimated and ground truth acceleration values over 1,000 s. Although they are largely overlapped, the curves inside the blue and green boxes are enlarged to highlight their differences. We see from the figure that the measurement of the quantum accelerometer (green curve) cannot follow the ground truth acceleration caused by the signal with wrapped phases. However, our proposed fusion process extends the dynamic range of the quantum accelerometer, and the
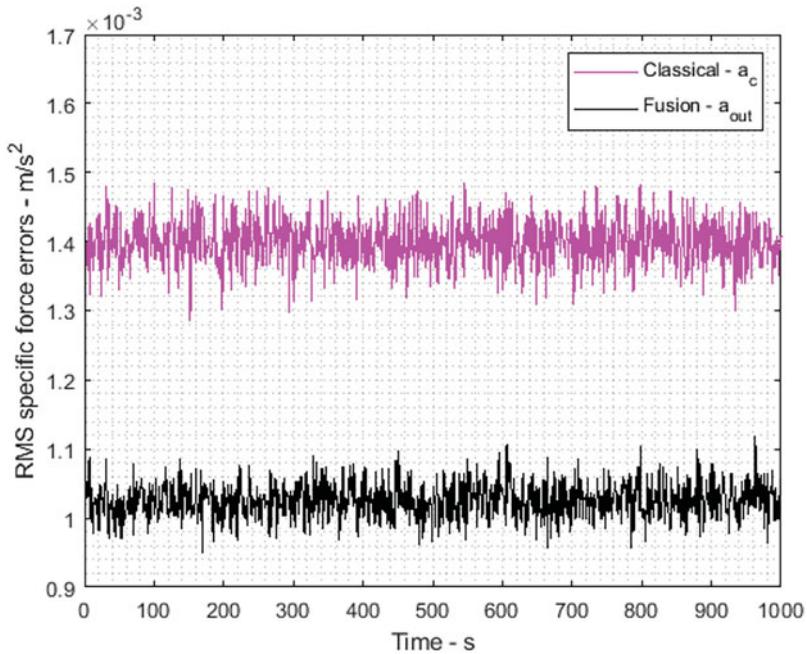
Figure 6. *RMS errors of specific forces versus time averaged over 1,000 runs. The equivalent standard deviation of white noise on the quantum accelerometer used in this simulation is $3 \cdot 1 \times 10^{-4} \, m \, s^{-2}$, and on the classical accelerometer is $2 \times 10^{-3} \, m \, s^{-2}$.*
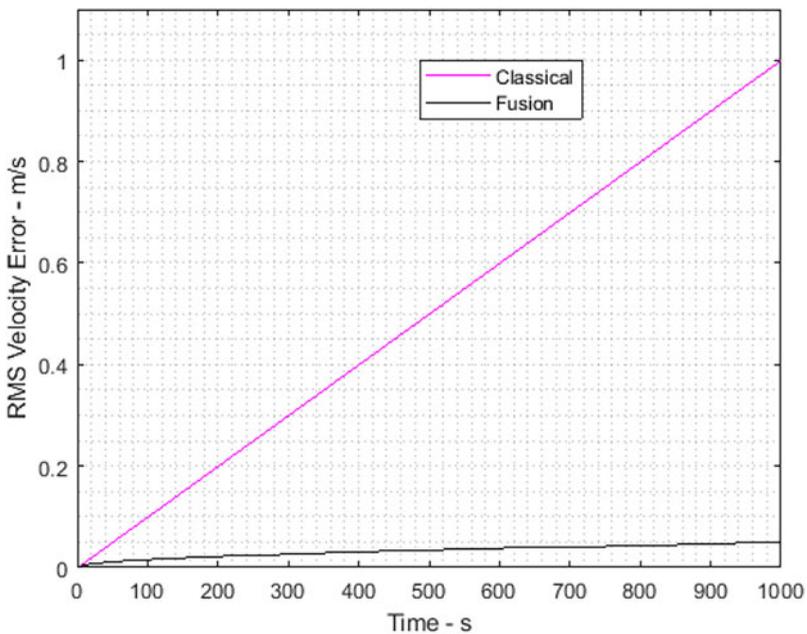

Figure 7. *RMS velocity errors versus time in the inertial navigation experiment averaged over 1,000 runs.*

output fusion signal (a_{out}) yields a smaller error than that of the classical accelerometer. The RMS error difference between classical (a_c) and fusion (a_{out}) specific force measurements with respect to ground truth are illustrated in Figure 6, which is computed from 1,000 Monte Carlo runs driven by a random
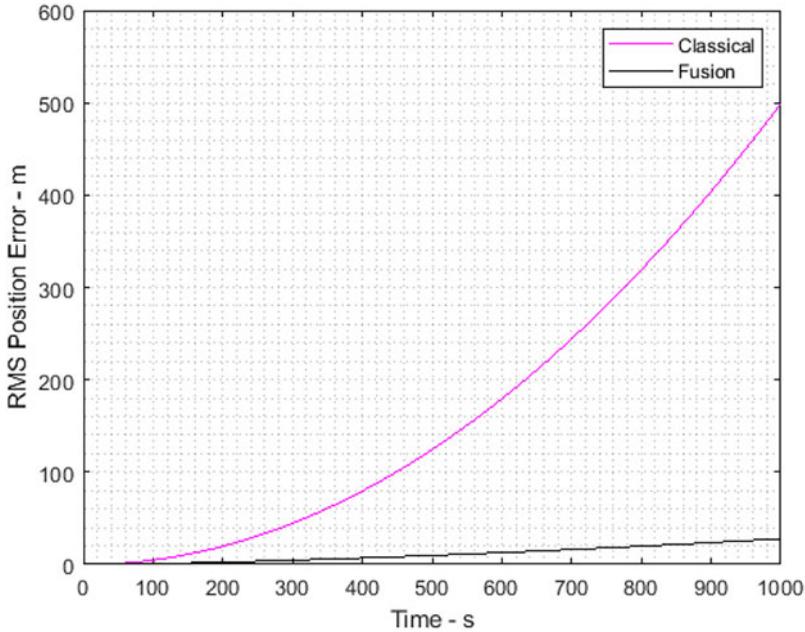
Figure 8. *RMS position errors versus time in the inertial navigation experiment averaged over 1,000 runs.*

acceleration profile. It shows that the proposed fusion process shown in Figure 2 is able to eliminate the bias and drift of the classical accelerometer by fusing ambiguity-corrected quantum accelerometer output.

The statistical results on the RMS velocity and position errors are shown in Figures 7 and 8, respectively. These results demonstrate a substantial improvement in velocity and position error performances in the inertial navigation scenario through the proposed fusion process over using the classical accelerometer alone.

Nevertheless, our experiments show that the fused acceleration error exists, and it increases with the scale of the underlying body specific force (see Figures 3 and 4). One major contribution to the fusion errors is from the mapping between the output signal S of the quantum accelerometer and the ambiguity-corrected quantum acceleration a_q, which presents different sensitivities due to the nonlinear nature of the sine function. Reading a_q from the linear part of the sine function in S can address the problem. This was shown by Bonnin et al. (2018), who used two orthogonal phased quantum accelerometers to remove the nonlinear sensitivity problem of the quantum accelerometer.

As shown in Figure 9 – a normalised plot for the expected output signal versus the value of acceleration – we assume that two 'exactly orthogonal phased' quantum accelerometers are available for the fusion process. At this stage, we assume that the output switching between the two quantum sensors is determined by selecting the normalised signal output which satisfies $S < N\sqrt{2}/2$, and that there is no switching error in the simulation. Enhanced error performances are observed from the simulation results similar to those shown in Figures 6 and 8 for the two orthogonal phased quantum accelerometer configurations. In addition, it is observed that the fusion error spread shown in Figure 3 is reduced by half with an orthogonal phased quantum accelerometer configuration.

It is worth mentioning that the errors of an inertial navigation system depend on many factors, and improving the performance of the accelerometers simply leads to other error sources dominating the inertial navigation performance, including gyro errors (Groves, 2008), gravity-modelling errors (Jekeli, 2012), sensor misalignment, bandwidth limitations and positive feedback of height errors through the gravity model (Titterton and Weston, 2004).
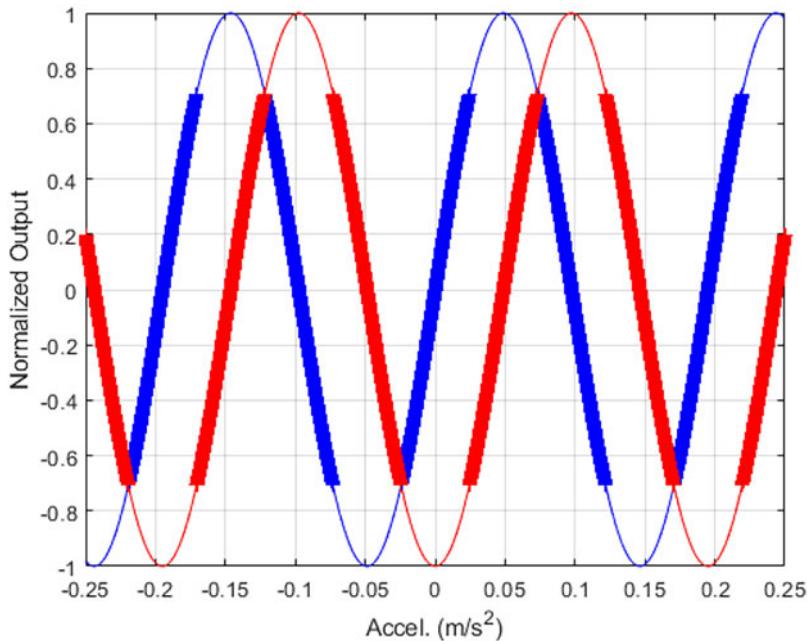
Figure 9. *Illustration of the normalised output signals of two orthogonal phased quantum accelerometers versus acceleration. The bold curve highlights the parts of linear sensitivity from the two sensors across the acceleration range, with $\phi_1 = 0$ (red) and $\phi_2 = \pi/2$ (blue).*

As ongoing research, we will continue our investigation along these lines for handling phase noise between the two orthogonal-phased quantum accelerometers, and simulating an adaptive phase-locked loop implementation for inertial navigation systems of predictable accelerations.

5. Conclusions

This paper proposes a fusion method that extends the dynamic range of a quantum accelerometer by unwrapping the signal phase of the quantum accelerometer output from the reading of a classical accelerometer using a maximum likelihood estimator. Consequently, the accumulative drift of the classical accelerometer is estimated using the output of the fusion process and is removed from the system output. The fusion algorithm enables the classical sensor to gain a substantially reduced drift over a dead reckoning navigation process. Promising performance is observed in the simulation results presented.

References

Battelier B., Cheiney P., Barrett B., Templier S., Gouraud B., Jolly O., Bouyer P., Porte H. and Napolitano F. (2020). A three-axis quantum accelerometer for mobile sensing applications. In: Franke-Arnold, S. (ed.). *Cold Atoms for Quantum Technologies*. SPIE. Available at: http://doi.ord/10.1117/12.2584181.

Bongs K., Holynski M., Vovrosh J., Bouyer P., Condon G., Rasel E., Schubert C., Schleich W. P. and Roura A. (2019). Taking atom interferometric quantum sensors from the laboratory to real-world applications. *Nature Reviews Physics*, **1**, 731–739. doi:10.1038/s42254-019-0117-4

Bonnin A., Diboune C., Zahzam N., Bidel Y., Cadoret M. and Bresson A. (2018). New concepts of inertial measurements with multi-species atom interferometry. *Applied Physics B*, **124**(9), 181.

Braasch M. (2015). *Inertial Navigation Systems*. Lecture Notes. USA: Ohio State University.

Butts D. L., Kinast J. M., Timmons B. P. and Stoner R. E. (2011). Light pulse atom interferometry at short interrogation times. *JOSA B*, **28**(3), 416–421.

Canciani A. (2012). *Integration of cold atom interferometry ins with other sensors*. Master's thesis, Second Lieutenant, Air Force Institute of Technology (USAF).

Carnal O. and Mlynek J. (1991). Young's double-slit experiment with atoms: a simple atom interferometer. *Physical Review Letters*, **66**, 2689–2692.

Cheinet P., Canuel B., Pereira Dos Santos F., Gauguet A., Yver-Leduc F. and Landragin A. (2008). Measurement of the sensitivity function in a time-domain atomic interferometer. *IEEE Transactions on Instrumentation and Measurement*, **57**(6), 1141–1148. doi:10.1109/tim.2007.915148

Cheiney P., Fouché L., Templier S., Napolitano F., Battelier B., Bouyer P. and Barrett B. (2018). Navigation-compatible hybrid quantum accelerometer using a Kalman filter. *Physical Review Applied*, **10**, 034030.

Cheiney P., Barrett B., Templier S., Jolly O., Battelier B., Bouyer P., Porte H. and Napolitano F. (2019). Demonstration of a robust hybrid classical/quantum accelerometer. In *2019 IEEE International Symposium on Inertial Sensors and Systems (INERTIAL)*. IEEE. Available at: http://doi.ord/10.1109/isiss.2019.8739762.

Chow R. (2011). Evaluating inertial measurement units. *Test and Measurement World*, 34–37, November 2011.

Close J., Kealy A., Moran B., Williams S., Haine S., Szigeti S., White A., Robins N., Freier C., Hardman K. and Legge P. W. S. (2019). *Cold atom sensing for inertial navigation systems - phase 1*. Technical report, ANU and RMIT, Australia, April 2019. Technical report, RMIT University, University of Melbourne and Australia National University.

Degen C. L., Reinhard F. and Cappellaro P. (2017). Quantum sensing. *Reviews of Modern Physics*, **89**, 035002.

Dutta I., Savoie D., Fang B., Venon B., Garrido Alzar C. L., Geiger R. and Landragin A. (2016). Continuous cold-atom inertial sensor with 1 nrad/s rotation stability. *Physical Review Letters*, **116**, 183003.

Freier C., Hauth M., Schkolnik V., Leykauf B., Schilling M., Wziontek H., Scherneck H.-G., Müller J. and Peters A. (2016). Mobile quantum gravity sensor with unprecedented stability. *Journal of Physics: Conference Series*, **723**, 012050. doi:10.1088/1742-6596/723/1/012050

Gillot P., Francis O., Landragin A., Pereira Dos Santos F. and Merlet S. (2014). Stability comparison of two absolute gravimeters: optical versus atomic interferometers. *Metrologia*, **51**(5), L15–L17.

Groves P. (2008). *Principles of GNSS, Inertial, and Multisensor Integrated Navigation Systems*. Boston: Artech House.

Hardman K. S., Everitt P. J., McDonald G. D., Manju P., Wigley P. B., Sooriyabandara M. A., Kuhn C. C. N., Debs J. E., Close J. D. and Robins N. P. (2016). Simultaneous precision gravimetry and magnetic gradiometry with a Bose-Einstein condensate: a high precision, quantum sensor. *Physical Review Letters*, **117**, 138501.

Jekeli C. (2005). Navigation error analysis of atom interferometer inertial sensor. *Navigation*, **52**(1), 1–14.

Jekeli C. (2012). *Inertial Navigation Systems with Geodetic Applications*. Berlin, Boston: De Gruyter, 2001. https://doi.org/10.1515/9783110800234

Keith D., Ekstrom C., Turchette Q. and Pritchard D. (1991). An interferometer for atoms. *Physical Review Letters*, **66**, 2693–2696.

Kim D. and Langley R. B. (2000). GPS ambiguity resolution and validation: methodologies, trends and issues. In *Proceedings of the 7th GNSS Workshop–International Symposium on GPS/GNSS, Seoul, Korea*. Volume 30.

Kitching J., Knappe S. and Donley E. A. (2011). Atomic sensors – a review. *IEEE Sensors Journal*, **11**(9), 1749–1758.

Lautier J., Volodimer L., Hardin T., Merlet S., Lours M., Pereira Dos Santos F. and Landragin A. (2014). Hybridizing matter-wave and classical accelerometers. *Applied Physics Letters*, **105**(14), 144102.

Li W., Wang X., Wang X. and Moran B. (2013). Distance estimation using wrapped phase measurements in noise. *IEEE Transactions on Signal Processing*, **61**(7), 1676–1688. doi:10.1109/TSP.2013.2238934

McGuinness H. J., Rakholia A. V. and Biedermann G. W. (2012). High data-rate atom interferometer for measuring acceleration. *Applied Physics Letters*, **100**(1), 011106.

McKilliam R. G., Quinn B. G., Clarkson I. V. L. and Moran B. (2010). Frequency estimation by phase unwrapping. *IEEE Transactions on Signal Processing*, **58**(6), 2953–2963.

Ménoret V., Vermeulen P., Le Moigne N., Bonvalot S., Bouyer P., Landragin A. and Desruelle B. (2018). Gravity measurements below 10^{-9} g with a transportable absolute quantum gravimeter. *Scientific Reports*, **8**(1). doi:10.1038/s41598-018-30608-1

Peters A., Chung K. Y. and Chu S. (2001). High-precision gravity measurements using atom interferometry. *Metrologia*, **38**(1), 25–61.

Quinchia A., Falco G., Falletti E., Dovis F. and Ferrer C. (2013). A comparison between different error modeling of MEMS applied to GPS/INS integrated systems. *Sensors*, **13**(8), 9549–9588. doi:10.3390/s130809549

Tennstedt B. and Schön S. (2020). Dedicated calculation strategy for atom interferometry sensors in inertial navigation. In *2020 IEEE/ION Position, Location and Navigation Symposium (PLANS)*. IEEE, 755–764.

Titterton D. and Weston J. (2004). *Strapdown Inertial Navigation Technology*. London: Institution of Engineering and Technology.